2019

Unusual Competitive and Synergistic Effects of Graphite Nanoplates in Engine Oil on the Tribofilm Formation

The Sang Pham
University of Wollongong, tsp310@uowmail.edu.au

Shanhong Wan
University of Wollongong, shanhong@uow.edu.au

Anh Kiet Tieu
University of Wollongong, ktieu@uow.edu.au

Ming Ma
Tsinghua University

Hongtao Zhu
University of Wollongong, hongtao@uow.edu.au

See next page for additional authors

Unusual Competitive and Synergistic Effects of Graphite Nanoplates in Engine Oil on the Tribofilm Formation

Abstract

To exploit the improved efficiency from formulated oil modified with graphite nanoplates (GNP), it is important to understand how GNP behave alongside conventional additives such as zinc dialkyl dithiophosphates (ZDDP). The results in this work demonstrate unusual tribological responses of engine oil due to GNP additions, which cannot be explained by the traditionally low shearing mechanism between graphene layers in GNP. A competitive and synergistic effect of GNP on tribofilm formation is proposed for this unusual friction and wear behavior. The presence of GNP modifies the tribofilm formation and spontaneously creates alternate hard and soft regions from the microscopic view of the surface. At low concentrations (≤0.05 wt%), graphene is formed by shear-assisted exfoliation of GNP and intermixed with intermediate oxide region. Due to its random orientation, graphene produces mechanical reinforcement of the tribofilm, but low shear yielding is not achieved. This gives rise to high friction but low wear conditions. At higher concentrations (>0.05 wt%), GNP align with their hexagonal sheets parallel to the surface to promote low-shear sliding, but wear increases. This is due to GNP clumping together which makes them less effective at forming graphene and providing stable reinforcement of the tribofilm.

Disciplines

Engineering | Science and Technology Studies

Publication Details

Pham, S. T., Wan, S., Tieu, K. A., Ma, M., Zhu, H., Nguyen, H. H., Mitchell, D. R. G. & Nancarrow, M. J. (2019). Unusual Competitive and Synergistic Effects of Graphite Nanoplates in Engine Oil on the Tribofilm Formation. Advanced Materials Interfaces, 6 (19), 1901081-1-1901081-14.

Authors

The Sang Pham, Shanhong Wan, Anh Kiet Tieu, Ming Ma, Hongtao Zhu, Hong Huynh Nguyen, David R. G Mitchell, and MItchell John Bromley Nancarrow

Unusual Competitive and Synergistic Effects of Graphite Nanoplates in Engine Oil on the Tribofilm Formation

Sang T. Pham, Shanhong Wan, Kiet A. Tieu*, Ming Ma, Hongtao Zhu, Huynh H. Nguyen, David R. G. Mitchell, Mitchell J. Nancarrow*

Sang. T. Pham, Dr. Shanhong. Wan, Prof. Kiet. A. Tieu, Dr. Hongtao. Zhu, Huynh. H. Nguyen
Faculty of Engineering and Information Sciences
University of Wollongong
Northfields Avenue, Wollongong
NSW 2522, Australia
Email: shanhong@uow.edu.au, ktieu@uow.edu.au
Prof. Ming. Ma
State Key Laboratory of Tribology
Department of Mechanical Engineering
Tsinghua University
Beijing 100084, China
Dr. David. R. G. Mitchell, Dr. Mitchell. J. Nancarrow
Electron Microscopy Centre
University of Wollongong
Squires Way, Wollongong
NSW 2522, Australia

Keywords: graphene nanoplatelets, graphene-based engine oil, interfacial tribolayer, graphene-reinforced oxide.

Abstract: To exploit the improved efficiency from formulated oil modified with graphite nanoplates (GNP), it is important to understand how GNP behave alongside conventional additives such as zinc dialkyl dithiophosphates (ZDDP). The results in this work demonstrate unusual tribological responses of engine oil due to GNP additions, which cannot explain by the traditionally low shearing mechanism between graphene layers in GNP. A competitive and synergistic effect of GNP on tribofilm formation is proposed for this unusual friction and wear behaviour. The presence of GNP modifies the tribofilm

formation and spontaneously creates alternate hard and soft regions from the microscopic view of the surface. At low concentrations (≤0.05 wt.%), graphene was formed by shear-assisted exfoliation of GNP and intermixed with intermediate oxide region. Due to its random orientation, graphene produces mechanical reinforcement of the tribofilm, but low shear yielding is not achieved. This gives rise to high friction but low wear conditions. At higher concentrations (>0.05 wt.%), GNP align with their hexagonal sheets parallel to the surface to promote low-shear sliding, but wear increases. This is due to GNP clumping together which makes them less effective at forming graphene and providing stable reinforcement of the tribofilm.

1. Introduction

Graphene is a friction modifier due to its unique two-dimensional structure with the basal plane layers held together by weak Van der Waals forces. Various methods have been used to synthesise graphene, e.g. wet chemical approach,[1] mechanical exfoliation,[2] vacuum arc technique,[3] etc. The addition of graphene to lubricating oil improves the thermodynamics and minimizes mechanical losses in machinery components through both friction and wear reduction, thereby improving energy efficiency.[4] Due to its densely packed and atomically smooth surfaces, graphene provides high chemical inertness, high strength, and easy shear capability, which contribute to its impressive tribological behaviour.[5] In addition, graphene has long been recognized as a solid or colloidal liquid lubricant by providing interlayer sliding interfaces with phenomenally low interfacial shear strengths.[6] However, the mechanisms for its performance as well as the nature of the tribofilm formation when graphene is added to fluid lubricant has not been fully established.

Numerous publications have reported that GNP with several graphene layers is a potential solid lubricant additive in pure oil base.[7] GNP can be mechanically exfoliated to form graphene or few layer graphene at the frictional interface. Due to its outstanding properties, these shear-induced 2D materials can potentially increase the lubricating efficiency of typical oil lubricant in terms of friction reduction and

wear alleviation. However, few works consider the effects of graphene on a formulated lubricant, especially if it is intended to be used as an additive for a fully formulated engine oil.[8]. As a result of the various additives in engine oil, the formation of an adaptive polyphosphate tribofilm is always present, which results from the tribochemical reaction between ZDDPs and iron/iron oxide on the solid surfaces.[9] Thus, the tribofilm dominates the sliding performance. The key problem is whether the presence of graphene/few-layer graphene will compromise the tribofilm effectiveness produced by such additives. Eswaraiah and co-workers investigated the lubricating effect of graphene in fully formulated oil.[8] They found that friction and wear characteristics of oil/graphene mixtures is concentration-dependent and proposed the corresponding nano-bearing effect of graphene. However, details on the exact mechanism when graphene becomes incorporated into the tribofilm and influences friction and wear in the presence of conventional oil additives are not fully understood.

It is worth noting that the interaction between nanoparticles and conventional additives of fully formulated oil intrinsically manage tribological performance of the tribofilm formation, via synergistic and antagonistic effects.[10] Additives based on metal dichalcogenides have been mainly used in formulated oil.[11] These dichalcogenides promote tribofilm formation and thereby improve the tribological performance of fully formulated oil. Rabaso et al. claimed that mixing inorganic fullerene nanoparticles (IF-MoS_2) did not affect the lubricating behaviours of a commercial oil significantly due to the presence of dispersants.[12] The presence of carbonaceous materials, e.g. carbon soot,[13] at the sliding interface exerts a remarkable influence on the resulting friction and wear. Zhou et. al proposed that diamond-like carbon can provide a catalytic effect enhancing ZDDP tribofilm formation, in which the tribochemical reactions between the ZDDP additive and the steel surface are accelerated by carbon species.[14]

Graphene/few-layer graphene are chemically and physically different to metal dichalcogenides and other carbon heterogeneities. In order to clarify the intrinsic relationship between macroscopic tribological

performance and graphene presence, reciprocating tribo-wear testing was carried out using a commercial engine oil mixed with GNP. In this study, we mainly consider the stressed-shearing effect on the tribofilm formation without much influence of temperature.[15] The focus is on understanding the effect of GNP additions on tribological capability and resultant tribofilm formation. To this end, all tests were performed at room temperature. Unusual tribological behaviour was observed, which is clearly different from published results related to graphene-based lubricating media.[7b-d, 8] SEM, FIB/TEM/EDS and Raman imaging techniques were applied to understand the surface/interface hierarchical evolution at micro/nano scale, and to explain how graphene, in the presence of conventional additives, influences tribofilm formation.

2. Results

2.1. Tribological behaviour of various lubricants

Using GNP-free oil to lubricate the steel-steel sliding contact at 20 N, resulted in a friction coefficient of approximately 0.17 in Figure 1a (the original values can be seen in Table S1), which is comparable with previous literature.[16] This value increases by about 7% when the concentration of GNP in the engine oil reaches 0.05 wt.% (G-B). Further increases in the concentration of GNP result in a slight decrease in the friction coefficient. Specimen G-E (0.5 wt.%) produces the lowest value of friction, being 1% lower than that of the base engine oil (graphene-free) test. These differences in friction coefficient in this study are not as significant as the reported results in the case of ultra-low addition of graphene materials[8]. However, in the case of wear, the opposite trend was observed. Both the plate and ball showed a distinguishable decrease in the specific wear rate with higher GNP content up to 0.05 wt.% (G-B). This specimen exhibits the lowest values of specific wear rate with 29% and 6% reduction for the plate and ball, respectively, in comparison to that of GNP-free engine oil. However, further increases in the concentration of GNP resulted in an increased wear rate. At the highest concentration (0.5 wt.%, G-E),

the plate and ball counterpart demonstrate a dramatic increase in wear by a factor of 5.5 and 3.0 respectively, compared to those of the base oil.

Figure 1b illustrates the important relationship between friction and wear for engine oil blends with various amounts of GNP. The region of low wear and low friction are the desired outcome. Compared to the base oil, lower specific wear rates were achieved for GNP concentration below 0.05 wt.%, albeit with a small increase in friction. This phenomenon is attributed to the smoothing and hardening effect of graphene/few-layer graphene on the sliding contacts. For engine oil with concentrations of GNP above 0.05 wt.% (G-C to G-E), friction was reduced with a higher concentration but the wear rates increased significantly. At the highest concentration (0.5 wt.%, G-E), wear increased dramatically, which is expected to cause the surface roughening. These values differ greatly from previously reported studies.[7c, 7d, 8] The established lubricating mechanism of graphene, namely that it gives rise to low shearing and low load bearing capability, does not adequately explain the results of the present investigation.

2.2. Wear morphology observation

The wear surface on the plate is relatively smooth for the contacts lubricated with base engine oil (Figure 2), without the distinct damage characteristics of ploughing, delamination and microgrooving. A few localised pores are present within the wear track. This lack of significant damage is attributed to the ZDDP tribofilm formation which inhibits wear.[9a] In terms of GNP-engine oil mixtures, the worn surfaces become smoother and the porous regions are mostly eliminated with G-A and G-B (Figure 2a). All tests with oil containing 0.05 wt.% GNP or lower result in relatively smooth wear scars. However, at the higher GNP concentrations (G-C to G-E), the sliding contacts show severe wear and roughened surfaces, with increased porous regions on the wear tracks (Figure 2a). In particular, abrasive wear is dominant in the case G-E, with features of micro-ploughing, formation of plateaux of compacted wear debris and delamination in Figure 2a. Higher concentrations of GNP undermine the performance of engine oil and thereby makes the surface quite rough, possibly due to the accumulation of flaky graphene and wear debries at the sliding interface.[7c, 7d]

The progression of wear on the ball counter part as a function of GNP content was very gradual (Figure 2b). Below the maximum GNP concentration, there was no evidence of ploughing and only minor roughening due to a small amount of surface spalls, producing a mildly pock-marked surface (Figure 2b). However, at the highest concentration of GNP, the severe wear results in the large scale transfer and compaction of wear debris. This leads to the formation of build-up plateaux of wear debris on the wear scar in the case of the sample G-E (Figure 2b).

2.3. Surface/Sub-surface compositional analysis

EDS mapping across the wear tracks lubricated with GNP-free engine oil, G-B (0.05 wt.%) and G-E (0.5 wt.%) lubricants are shown in Figure 3. Some locations enriched with carbon can be identified, which is associated with either GNP aggregation or amorphous carbon from the decomposition of oil molecule during friction. This can be further confirmed by the Raman analysis in Figure 4. Zinc, phosphorus, sulfur, and oxygen elements are identified, these coming from the oil additives. This indicates the presence of zinc polyphosphate/sulfide compounds on the frictional surface. From the elemental mapping images, zinc, sulfur, oxygen and phosphorus are preferentially located at the ridge and valley regions within the wear track, which is consistent with the tribofilm topography reported by Warrant et al.[17] As more GNP is blended within engine oil, the distribution of elements (Zn, P, and S) from oil additives within the wear track becomes non-uniform as shown in (Figure 3b-3c). This indicates that the GNP addition interferes with the dynamically-formed ZDDP-based tribofilm at the frictional interface.

The use of Raman mapping in this study focused on the identification of GNP and graphene/few-layer graphene within the wear track (Figure 4). Three distinct peaks at 1335 (D peak), 1580 (G peak), and 2660 cm^{-1} (2D peak) were encountered in the wear tracks lubricated by base engine oil, G-B and G-E. For engine oil, the broad D and G peaks are attributed to the appearance of amorphous carbon while the broad 2D peak corresponds to the vibration of polymeric hydrocarbons.[17] Regarding G-B and G-E, the D, G and 2D peaks are sharper and narrower. Those results indicate the presence of graphene within the wear track in these samples. The I_D/I_G ratio of both G-B and G-E experiences a significant increase

compared to that of pristine graphene powder (0.83) with 1.14 and 1.80, respectively. This is attributed to the structural transformation of the GNP during sliding by converting it to a partially disordered graphitic structure.[18]

Raman spectroscopy with imaging is an effective technique for studying graphene,[19] as it can locate the position of graphene within the complex matrix.[20] Thus, Raman mapping is applied inside the wear track to accurately assess the locations of formed graphene (Figure 4). Since In both wear tracks, the D and G bands maps identify carbon-rich areas in localised regions. The G-B (0.05 wt.% GNP) specimen displays traces of fine graphene particles within the wear track in Figure 4b, while relatively large GNP are clearly visible for the lubricant test of G-E (0.5 wt.% GNP) in Figure 4c. The results indicate that graphene/few-layer graphene or GNP being preferentially located in the smooth regions, which is in good agreement with SEM/EDS mapping analysis.

The intense oxide peak at 682 cm^{-1} is related to Fe_3O_4 in Figure 4,[21] and small amounts of FeS and FeS_2 are identified in Figure S5, where the peak at 371 cm^{-1} can be attributed to FeS_2 formed during sliding.[22] The weak peaks at 1000 cm^{-1} are assigned to P-O bonds, which indicates the trace of polyphosphate formation under the stressed shearing condition (Figure S5).[23] These results show that Raman analysis is an effective tool for indentifying graphene and zinc polyphosphate compounds present within sliding contacts.

2.4. Effect of graphene addition to the tribofilm growth

The cross-sectional images of the tribofilm on the worn surface (taken perpendicular to the wear track) are displayed in Figure 5. In the cases of G-B (0.05 wt.%) and G-E (0.5 wt.%), FIB sampling was conducted in two different regions: 1) porous region with high concentration of ZDDP (Area 1); and 2) smooth region (carbon rich) region (Area 2). STEM bright field images of the base oil, G-B and G-E specimens all show a strong diffraction contrast in the deformed steel, and much lower contrast in the quasi-amorphous/nanocrystalline tribofilm. The layers above the uppermost dashed line (original

surface) are platinum layers deposited during FIB specimen preparation, to protect the surface from the Ga ion beam. The extent of the tribofilm outlined with dashed lines shows highly variable thickness. Area 1 represents the porous regions which are rich in ZDDP, and here the tribofilm is thickest (up to 120 nm). Meanwhile, Area 2 represents the carbon-rich (ZDDP-poor) regions and here the tribofilm is thinnest (around 20 nm).

The tribofilm derived from the engine oil is continuous and relatively uniform, with a thickness of 30-50 nm. In the case of G-B and G-E lubricants, it is noticeable that the thickness of the tribofilm differs significantly between Area 1 and Area 2. The tribofilm in the rough, porous region (Area 1) is quite variable in thickness and is typically thicker (30-120 nm) than that obtained by base engine oil (30-50 nm). However, the tribofilm formed in the smooth regions of the wear scars (Area 2, carbon-rich, ZDDP poor) is significantly thinner, around 20 nm. The typical tribofilm thickness in G-B (0.05 wt.% GNP) is thicker than that in G-E (0.5 wt.% GNP) at the Area 2, while the tribofilm grows thicker in the porous region (Area 1) in the case of higher concentration of GNP. Thus, blending GNP within engine oil changes the tribofilm uniformity across the wear track.

2.5. Analysis of hierrachically-structured tribofilm

The tribofilm formed under base oil lubrication (GNP-free) is heavily deformed (Figure S7). STEM high angle annular dark field imaging (HAADF) in Figure 6a and the corresponding EDS line analysis in Figure 6c highlight the laminated hierarchy of the tribofilm produced by base engine oil. Similar structures have been reported in the literature.[24] The contrast of STEM-HAADF images varies as an approximate function of thickness and Z^2 where Z is the mean atomic number. Low atomic number regions therefore appear dark in such images. High resolution imaging indicates that dark tribofilm layer is almost entirely amorphous. EDS analysis shows large amounts of zinc and calcium to be present in the intermediate layer 1, which arise from engine oil additives (Figure 6c). The intermediate (brighter) layer 2 between the tribofilm and the deformed metallic region, contains a significant amount of sulfurn, iron

and zinc (Figure S7) from ZnS and FeS, and similar observations have been made elsewhere.[24] In addition, the high manified STEM-BF pictures in Figure S7 indicate the presence of crystalline structure from FeS_2 (211) (d-spacing = 0.18 nm)[25] and ZnS (220) (d-spacing = 0.196 nm)[26], which correspond to the regions with strong EDS mapping signal of zinc, iron and sulphure (Figure S7).

The EELS spectrum of the carbon K-edge (Figure 6b) taken from the boxed region in Figure 6a, confirms the presence of carbon and permits its bonding state to be assessed. The carbon K-edge comprises a sharp peak at around 285.5 eV (π*) followed by a broad peak ranging from 290 eV to 300 eV (σ*), which is explained to be the transition from the core 1s state to the π* state and σ* state, repectively.[27] In Figure 7b, the ratio of $I_{\pi^*}/(I_{\pi^*}+I_{\sigma^*})$ is found to be 0.094 with the relative sp^2 bonding fraction as 32%, which indicates the dominant sp^3 coordination of carbon within the amorphous polyphosphate tribofilm matrix. Given that this specimen was derived from the base engine oil, this amorphous carbon must originate from the decomposition of oil.

STEM-HAADF images of G-B (0.05 wt.% graphene concentration) specimen reveals a uniformly thin tribofilm at the carbon-rich and smooth region (Area 2) in Figure 7a. Corresponding EDS mapping in Figure S9 confirms that this thin tribofilm comprises mainly iron oxide with low concentration of sulphur, phosphorus and zinc originating from oil additives. An EDS line scan (yellow arrow in Figure 7a) acrross the tribofilm in (Figure 7c) reveals that sulphur are concentrated in the middle region (Intermediate layer 2) of the tribofilm rather than at the top and bottom. It corresponds to the formation of zinc/iron sulfide compouds. The thickness formation of the polyphosphate tribofilm is not significant as compared with that of the GNP-free engine oil. However, there is no detectable fringe of the graphene/few-layer graphene inside tribofilm by STEM- HAADF imaging.

A nine point EELS line scan was performed across the tribofilm in Figure 7d to invesitigate the state of the carbon. The corresponding bond fraction of sp^2-C within the tribofilm is shown in Figure 7e. From spot 1 to spot 4, the $I_{\pi^*}/(I_{\pi^*}+I_{\sigma^*})$ ratio ranges from 0.19 to 0.18, which corresponds to the bond fraction

of 63-66%. It is significantly higher than the value of 32% from engine oil. This suggests the presence of some sp^2 ordered carbon within the superficial region of the tribofilm, probably due to graphene/few-layer graphene. The ratio in spots 5 to 6 in contrast demonstrates a significant decrease in the sp^2-C bond fraction to 35%. However between spot 6 and 9 , the sp^2-C bond fraction increases dramatically again to 96%, which suggests the presence of sp^2-bonded carbon materials near the interface with the deformed metallic region.

The dense-oxide tribofilm is shown as the red boxed region in Figure 7a and 7b, which displays the compaction region (lower zone outlined by red dashed lines in Figure 7a) below the ZDDP tribofilm. In particular, the fine scale of folded fine graphene/few-layer graphene particles are observed in the bright field image of this area (Figure 7b). The sp^2-C bond fraction calculated from the EELS C K edge (Figure 7e) confirms graphene/few-layered graphene being involved within this consolidated layer. From point 7 to 9, the intensity of π^* peak at 285 eV is close to the σ^* peak at 290 eV. The corresponding bond fraction of sp^2-C at these points are ~79-96%. Moreover, the EELS of other elements (Figure S14) demonstrated that the consolidated layer was formed by iron oxide. In contrast to the underlying iron base with a highly crystalline character, the incorporation between graphene and the iron oxide is evident by the presence of finely compacted structure (Figure 7b). It is concluded that GNP were exfoliated into graphene/few-layer graphene during shearing conditions. These particles subsequently dissociate into fine particles during the stressed-shearing operations. The resulting fine particles partly compacted with the iron oxide and form a reinforced layer by the mechanical shearing. Qualitatively hardness measurements (Figure S13) showed the strenghthening effect of GNP additions on the tribofilm in the smooth area in the sample G-B, as a result of the formation of graphene/iron oxide composite layer.

HAADF imaging at the carbon-rich region (Area 2) for test G-E (0.5 wt.% GNP concentration) is shown in Figure 8a. There are some slight differences in the hierarchy of the tribofilm compared to that for the G-B specimen. The tribofilm at the interface comprises of two main feartures:1) carbon-rich layer and 2)

ZDDP-concentrated layers. An absence of the compacted oxide tribofilm is apparent in Figure 8b. The carbon-rich layer in this specimen is much thicker (~30 nm), while the intermediate ZDDP tribofilm is thinner (≤ 5 nm) (Figure 8b) than the one developed in G-B (Figure 7a). The bright field image (Figure 8b) shows large GNP arranged with their basal planes parallel to the original surface, near the base of Intermediate Layer 1. The EDS line scan (marked by a yellow arrow in Figure 8a) reveals that phosphorus, sulfur and zinc become more concentrated at the intermediate region of the tribofilm. Meanwhile calcium related compounds are mainly located at the top layer, which is somewhat analogous to the result obtained from engine oil and G-B.

To prove the presence of graphene/few-layer graphene or GNP in this region, an EELS line scan across the tribofilm at 10 positions indicated in Figure 8a was carried out. The C-K edege spectra from spots 1 to 7 are quite similar to each other, and the bond fraction of sp^2-C is relatively constant, around 60%. This compares with a much lower value of 32% for the equivalent region formed by engine oil. Thus, it suggests a high concentration of GNP particles is present. A spike in the $I_{\pi^*}/(I_{\pi^*}+I_{\sigma^*})$ ratio of 0.22 with the associated sp^2-C bond fraction of 78% was found at spot 8 (Figure 8d and 8e). This corresponds to the region containing stacked GNP (Figure 8b). In the G-E case, the high concentration of GNP in lubricant (0.5 wt.%) results in high concentration of highly dispersed few/multi-layer graphene through the tribofilm, in addition to clusters of sheets. Such concentrations can be detected by EELS, and also by bright field STEM imaging, but only when the cluster are oriented such that the beam is parallel to the basal planes-which produced strong scattering.

3. Discussion

The present study attempts to understand the competitive and synergistic mechanism of graphene on tribofilm formation in relation to unusual tribological performances. Generally, ZDDP additives are capable of controlling wear and inhibiting oxidation. They reduce wear by the spontaneous deposition of an adaptive polyphosphate tribofilm that is responsive to variations in the ambient conditions.[28] The

hard and soft acids and bases (HSAB) principle[9a] explains the continuity of the tribofilm formed under tribological contacts due to tribochemical reaction between polyphosphates and the iron oxides. In this study, Raman and STEM highlighted the presence of polyphosphate and metallic sulfide compounds in the tribofilm (Figure 6-8), and the tribofilm demonstrated the laminated hierachy in which both composition and film structure vary.

In this study, the spatial analysis of the composition and structure of the tribofilm was focused rather than the chemical characterization by XPS. In particular, the location of GNP and their interaction with surrounding media at the frictional interface are mainly considered. A large number of publications have reported the chemical characterization of polyphosphate and sulphide compounds by XPS in terms of the binding energies and the atomic ratio of the tribofilm.[24, 28-29] The components variation and structural transformation within the tribofilm can be also studied by XPS at different testing conditions, e.g. temperature, loading and speeds, albeit with quite low spatial resolution. In this study, aberration-corrected STEM/EDS/EELS analysis was used to provide high resolution spatial chemical and structural characterization, which greatly surpass the capabilities of XPS.

Higher temperature facilitates an increase of the tribofilm formation rate,[29a, 29b, 30] but does not affect significantly on the overall steady state film thickness.[31] Although temperature influences the fine structure alteration and the compositional migration of the tribofilm,[9a] the ZDDP tribofilm can be formed on rubbed surface even at room temperature.[29a] In particular, the formation of long-chain polyphosphate on the ZDDP tribofilm is favorable at elevated temperatures (>80^{o}C),[29a] relative to room temperature. However, as this study aims to clarify the influence of GNP additions on resultant properties of the tribofilm, all testing was done at room temperature. In this case, the presence of graphene indeed leads to the structural alteration of the tribofilm at the nanoscale. Although the friction was not influenced significantly as expected at macroscopic scale, its effect on frictional behaviour is still evident (Figure 1a). GNP additions to engine oil promoted a significant wear resistance, as shown in Figure 1a.

Extensive studies of graphene-based materials as an additive to both pure oil[7b, 7c, 32] and engine oil[8] have been reported. Appropriate graphene addition results in optimal friction and wear performance of oil media under specific conditions, due to its intrinsic low-shearing nature.[8] However, no studies have directly addressed the location and structure of graphene between the sliding contacts. In the present work, unusual friction and wear behaviour were encountered (Figure 1a and 1b), which appears to contradict previous studies.[7c, 7d, 8] Thus, existing mechanisms of graphene-based materials at the sliding contact cannot fully explain the tribological performance in this study. Some new findings regarding how graphene materials interact with conventional additives are given on the basis of the hierarchical characterization of the tribofilm by using STEM/EDS/EELS techniques.

It is proposed that under the stressed-shearing conditions, a composite structured surface with a combination of elasticity and plasticity is formed spontaneously across the rubbing surface. Self-segregation of shear-induced graphene and additives from the oil base occurs. Graphene has extremely high mechanical strength and elasticity which can suppress wear at the contacting interfaces,[5] while polyphosphate compounds are very plastic and relatively soft. The tribofilm is thinner in the smooth areas and thicker in the porous regions - herein called Areas 2 and 1 (Figure 5), respectively. It is clear that the formation of graphene/few-layer graphene at the interface interferes the tribofilm development in terms of the uniformity of the tribofilm across the wear surface and the structural hierarchy evident in the cross-sectional view.

The tribofilm derived from base engine oil demonstrates good uniformity and continuity over the intermediate oxide layer of steel in Figure 6. In contrast, GNP additions lead to an alteration of the hierachical arrangment of this tribofilm as shown in Figure 7 and 8. In particular, the reactive polyphosphate layer becomes thinner for test G-B (10 nm) and test G-E (5 nm) at the smooth region (Area 2). It is deduced that GNP may retard/block the formation of polyphosphate tribofilm in the areas enriched with graphene/few-layer graphene. As shown in Raman mapping in Figure 4b-4c, partial coverage of such surfaces with clusters of GNP and/or graphene can be identified. Thus, graphene

clustering and ZDDP film formation are competitive process, indicating an antagonistic relation between graphene and additives in oil.

At low concentrations of GNP (G-B-0.05wt.%), the thin ZDDP tribofilm (~15 nm) in Figure 7 shows low concentrations of elements originating from engine oil additives like ZDDP in comparison to base engine oil (Figure 6). GNP were exfoliated into graphene/few-layer graphene during shearing conditions. These particles subsequently dissociate into fine particles during the stressed-shearing operations. The resulting fine particles partly compacted with iron oxide, and form a reinforced layer by the mechanical stressed-shearing. This consolidated oxide layer enhanced the mechanical strength of the contacting surface, which is consistent with the mechanical enhancement of graphene scrolling orientation in the composite materials.[33] The mechanial enhancement of graphene additions in metallic bulk and epoxy resin is well known.[34] In this situation, graphene/few-layer graphene particles will be entrapped across the tribofilm layer due to the pressure/shearing-induced intermixing effect, enabling the mechanical reinforcement of tribofilm (Figure 7 and 8).

To demonstrate the mechanical reinforcement effect, nanoindendation hardness measurement within the wear track was obtained for the smooth region (carbon rich area) and steel base (Figure S12-S13). It should be noted that the nanoindentation test was performed to demonstrate qualitatively the effect of graphene on the strength of the third layer of oxide scale. The results did not account for the effect of piles-up nor viscoelastic properties, which are complex topics for multi-layer thin films, and thus beyond the scope of this paper. An average hardness of ~4.75 GPa in the steel base is obtained in different contact depths (Figure S12d), while the smooth region shows a much higher hardness of ~8.50 GPa (Figure S13a). It is noted that the values obtained in the smooth area are the global measurements for the main ZDDP tribofilm and the underlying consolidated oxide layer. These results suggest the mechanical reinforcement of the tribofilm due to graphene presence in the consolidated oxide region, which enhances wear resistance. Nevertheless, it causes a slight increase in friction (Figure 1a). This is consistent with the improved mechanical properties observed in amorphous carbon and diamond-like carbon embedded

with nanoparticles.[35] The addition of GNP modifies the tribofilm formation of engine oil, which spontaneously creates the alternate hard and soft regions within the wear track surfaces.

However, STEM-BF imaging did not detect any single sheet crystalline graphene. This does not mean that they were not present, simply that they could not be detected. Many experimental aspects make imaging single sheet graphene extremely difficult, including: very weak scattering of electrons by carbon; deformed and randomly oriented sheet of graphene in an otherwise amorphous matrix; large foil thickness (~100 nm) relative to the graphene particle dimension. Only regions of several sheet, heavily deformed graphitic sheets were identified (Figure 7), and only those with their basal-plane parallel to the electron beam would scatter strongly enough to be imaged. Dravid and co-workers reported that the EELS carbon K edge peak ratios serves as a good indicator of graphite crystal orientation.[36] This means that the measured EELS peak ratios (Figure 7e) are the composite value for randomly oriented graphene combined with any amorphous carbon which may be present. Such values would always be intermediate between those of pure amorphous carbon (low values) and graphene (high values-in the case of beam parallel to the basal plane).

In the case of G-E (0.5 wt.% GNP), the GNP particles tend to form the large clusters as reported previously.[7a, 7c] Stacked multilayer GNP (Figure 8) and finely exfoliated graphene/few-layer graphene incorporated into the surrounding structure (oxide tribolayer and tribofilm) (EELS spectrum in Figure 8) were observed. The stacking phenomena facilitates friction reduction compared to that of G-B, due to the intrinsic Van der Waals force between each layer.[5] This is the case where the basal plane of graphene layer is oriented parallel to the shear force. It is speculated that the GNP or graphene/few-layer graphene are incorporated increasingly into the tribofilm at higher concentrations. Due to a large population of GNP particles in the tribofilm at high concentrations, there is a random orientation with a fraction aligned parallel to the shear direction. This eventually reduces the friction compared to that of G-B (0.05 wt.% GNP).

However, the presence of low shear strength from graphene layer means that the structural integrity of the tribofilm was destabilized with increasing concentration of GNP. Due to the inherent chemical incompability between tribofilm components and GNP, unfavourable structural assembly across the tribofilm takes place at high additions of GNP.[37] In particular, high concentration of GNP entails the agglomeration effect among these particles, which in turn deteriorates the uniform distribution of exfoliated graphene within the tribofilm. The reinforcing effect of graphene/few-layer graphene on the tribofilm consequently does not occur. It is clear that the intermediate oxide region in specimen G-B (0.05 wt.%) contained an intimate mixed composite of oxide and graphene, which is absent in the case of higher concentrations specimen G-E (0.5 wt.%). This lack of consolidated oxide film conversely undermines the wear resistant capability of tribofilm and thereby wear aggregation. Conclusively, high GNP concentrations makes the intermediate ZDDP tribofilm layer thinner, and does not create a consolidated oxide tribo-layer at the sliding interface. Figure 9 shows a schematic illustration of the nature of the tribofilm, highlighting the competition and synergy between graphene and ZDDP in response to hierarchical tribofilm formation in the graphene-poor (Area 1) and graphene-concentrated (Area 2) regions.

On the other hand, the formation of the ZDDP tribofilm is much thicker in Area 1 in both cases of low (G-B, 0.05 wt.%) and high (G-E, 0.5 wt.%) additions (Figure 5). The tribofilm thickness reaches 120 nm for G-B and G-E as compared to that derived from graphene-free engine oil (50 nm). Based on the study of Zhou et al.[14], GNP may have an effect to ZDDP tribofilm formation. This effect is predicted that accelerate the chemical reaction between ZDDP and steel substrate. Carbon with both sp^2 and sp^3 hybridizations also produces a catalytic effect on oxygen insertion reaction and oxidation dehydrogenation, respectively.[38] In the present study, a rise in I_D/I_G ratio in Raman (Figure 5) verifies the GNP dissociation with the increase of defects on the graphene surface, leading to the evolution of abundant edges which are highly reactive to other components.[39] In addition, the conjugated π electron of the sp^2 system on the graphene structure facilitates the electron transfer process,[38] which may

accelerates the decomposition of ZDDP to Zn^{2+} and DDP^{-} and increases the growing rate of polyphosphate tribofilm.

The unusual tribological behaviour in the present study may also be related to the contributions from the amphiphilic additives like dispersant and detergents. Rabaso and co-workers reported that the excessive dispersants prevent the agglomeration of IF-MoS_2 nanoparticles in the lubricant.[12] However, they degrade the adhesion between these fine particles and steel substrate and prevent the low-friction tribofilm formation. In our investigation, such dispersants and detergents are certainly present in the commercial engine oil, which may impair the effectiveness of GNP additions at reducing friction (Figure 2). The STEM-EDS spectrum (Figure 7-9) confirms the presence of calcium within the tribofilm that is undoubtedly related to calcium carbonate and calcium-based detergents.[40] However, this study has focus on the relationship between the unusual tribological behaviour and the interaction of graphene and typical ZDDP during the formation of hierarchical tribofilm. The influence of dispersants on tribological response will be not covered in this study.

4. Conclusions

The unusual friction and wear behaviour of GNP-based fully formulated oil has been investigated, and the results obtained are significantly different compared to previous reports in the literature. Low concentrations of GNP improved wear resistance but increased friction, and high concentrations resulted in increased wear but lower friction. A synergistic and competitive interaction between graphene and the tribofilm formation is proposed to be responsible for the unusual tribological performance. GNP may enhance the rate at which tribofilms develop, in surface regions with low local graphene concentrations. However, in regions where the surface graphene concentration is high, the graphene blocks tribofilm formation. At low concentrations, graphene becomes incorporated into the growing tribofilm and mechanically reinforces it to produce of a composite oxide region. This contributes to slightly increased friction but decreased the wear behaviour of this tribofilm. In contrast, high additions of GNP result in a

friction reduction due to the formation of a tribofilm containing a significant fraction of stacked GNP along with very finely dispersed graphene. This low shear film contributes to the friction reduction, but leads to a dramatic increase in wear. It may be due to a non-uniform distribution of graphene/few-layer graphene resulting from aggregation of these particles within the formed tribofilm. The aggregation phenomena between GNP particles in turn leads to disruptive and destabilized effect to the hierarchical structure of the tribofilm formation. This study has shed a new light on the complexities of developing and using GNP-base fully formulated oil lubricants for automotive and related applications.

5. Experimental Section

Preparation of test lubricant: Graphite nanoplatelets (GNP) were used as the frictional modifier without further modification in this study. GNP were purchased from the Sixth Element Materials Technology Co. Ltd (Changzhou, China). Atomic force microscopy (AFM) (Figure 10a) demonstrates a stack of few layers of graphene with the thickness range of 2-5 nm and an approximate diameter of 500 nm, which is suitable with the term of graphite nanoplatelets (GNP).[41] Transmission electron microscopy (TEM) bright field imaging (Figure 10b) reveals a clear lattice fringes from a wrinkled graphene sheet with crumpling and scrolling presence. This specific morphology provides a very high specific surface area of graphene that enhances its dispersion in lubricating oil[42]. The corresponding selected area electron diffraction pattern (SAED) shows a weak diffuse ring with the intense spot patterns, due to the inherent crystalline nature of graphene. The diffraction patterns correspond to the reflections from $(10\bar{1}4)$, $(10\bar{1}1)$ and $(10\bar{2}1)$ planes in the graphite structure. Raman spectrum (Figure 10c) further shows three prominent peaks at 1335 cm^{-1}, G band at 1584 cm^{-1} and specific 2D at 2660 cm^{-1} with the ratio of I_D/I_G equal to 0.83, which is consistent with highly crystalline graphene sheets which are stacked randomly[43].

The oil base for lubrication was a commercial engine Armour 10W-30 Synthetic oil (Valvoline). This type of oil has a density of 0.86 g/cm^3 at 15.6^oC. Its dynamic viscosity was equivalent to 77.1 cSt (40^oC) and 11.6 cSt (100^oC), respectively. The concentration of ZDDP was approximately 800 ppm in test

engine oil[44]. In this study, this engine oil was used as the base oil, which was ultrasonically blended with the defined amount of graphene for the preparation of formulated engine oil containing graphene. The graphene-engine oil mixture was prepared by dispersing an appropriate amount of graphene nanoplatelets in the engine oil base by using a magnetic stirrer at 1000 rpm, and followed by the ultrasonication for 4 hours, where the temperature was kept at 30^{o}C within the cooling water bath. Prior to each test, the formulated specimens was re-dispersed in an ultrasonic bath in 30 minutes to minimise any potential settling and agglomeration of the particles. Figure 10d shows the final lubricant specimens after mixing with various amount of GNP. The dispersion are quite stable as there is no obvious phase separation after one week.

Steel sample preparation: A 316 stainless steel (SS16) ball of 6.35 mm diameter was selected as the stationary part with an initial roughness of Ra = 0.127μm and a hardness 25-39 Rockwell C. A stainless steel (SS04) (hardness 25-39 Rockwell C) was chosen for the sliding element with the dimension of 115×40 ×3 mm^3, and an initial roughness of Ra = 0.45μm. The composition of the ball and plate are given in the Table 1. Both steel components were ultrasonically cleaned by ethanol and acetone for the removal of contaminants.

Friction and wear testing: The wear and friction testing were conducted in the BICERI pin-on-plate reciprocating equipment. The pin was a stainless steel ball and the counter-face was rectangular stainless steel plate. The normal load of 20 N corresponding to a maximum Hertzian pressure of 1.61 GPa, sliding velocity of 0.13 m$*$s^{-1}, and total sliding distance of 4800 m were applied for all tests. In this study, a stressed-shearing effect on the tribofilm formation was mainly investigated and the influence of temperature was not considered[15]. All the tests were performed at room temperature to simulate the cold-start conditions of engine. Prior to each friction test, 1 ml of the formulated engine oil containing graphene was dropped on the steel plate surface. The friction coefficient was recorded using the load transducer KD40s ± 20 N with the accuracy class of 0.1%. After sliding assessments, the plate and ball

were cleaned with ethanol solution to remove the debris and oil residue for subsequent analysis. It is expected that a boundary lubrication regime occurs for all the friction tests in this study. The minimum oil film thickness (h_{min}) and the dimensionless ratio (λ) were speculated on the basis of the equations proposed by Dowson-Higginson[45].

$$H_{\min} = 3.63U^{0.68}G^{0.49}W^{-0.073}(1-e^{-0.68k}) \quad (1)$$

$$h_{\min} = H_{\min}.R \quad (2)$$

$$\lambda = \frac{\eta_{\mu\nu}}{\sqrt{P_{0,\alpha}^2+P_{0,\beta}^2}} \quad (3)$$

$$U = \frac{\eta_o.u}{E'.R} \quad (4)$$

$$G = E'.\alpha \quad (5)$$

$$W = \frac{F}{E'.R^2} \quad (6)$$

Where η_o is the dynamic viscosity of oil (0.067 N s m^{-2}), *u* the linear velocity (0.13 m s^{-1}), *E'* equivalent modulus of elasticity (2.119.e^{11} N m^{-2}), *R* radius of the ball (0.00325 m), α pressure viscosity coefficient (2.03 e^{-8}) and *F* is the external load (20 N). *k* is the ellipticity parameter equal to 1. The minimum film thickness ($h_{\min}$) is 40.59 nm and the lambda ratio (λ) is 0.15, which is much lower than 1. Boundary lubrication was therefore achieved during this frictional testing.

Scanning Electron Microscopy (SEM): After the friction test, the morphologies of the worn surfaces were examined by using Scanning Electron Microscopy (SEM) (JEOL JSM-6490LV, Japan) coupled with Energy Dispersive X-ray Spectroscopy (EDS) at different locations. 15 keV accelerating voltage was employed to image topographies using secondary electron imaging (SEI) mode. Backscattered electron imaging mode (BED) at the same accelerating voltage was used to identify chemical composition variations in the near-surface region using a working distance of 10 mm.

3D Optical Profilometer: Wear volumes were determined by first carefully washing components in ethanol multiple times. Ball loss volume were derived from measurement of the wear scar diameter while

the corresponding groove volume on the wear track of the plate was measured by a 3D Optical Microscope (ContourGT-K, Bruker). In the disc wear track, four different positions along the wear track were recorded and then the wear morphology profile were exported for the wear area calculation. The cross-sectional wear area was calculated by using Origin software to get a mean wear area. The wear area was then multiplied with the wear track length to determine the wear volume. In the case of ball, wear diameters in different tested balls were recorded and used for calculating the wear loss volume based on equation (7), where d is wear scar diameter and r is ball radius. The wear rate in both counterparts can be calculated from the wear volume as indicated in equation (8):

$$\text{Ball volume loss} = \left(\frac{\pi h}{6}\right) * \left[\frac{3d^2}{4} + \left(r - \left(r^2 - \frac{d^2}{4}\right)^{\frac{1}{2}}\right)^2\right] \qquad (7)$$

$$\text{Specific wear rate} = \frac{\text{Volume of wear track}}{\text{Applied load} * \text{Sliding distance}} \qquad (8)$$

Raman Spectroscopy: A LabRam HR 800 Raman Spectrometer (Jobin Yvon, Horiba) with 3 μm spot size and 1065 nm laser line was used on the powdered particles. In addition, Raman spectra and Raman imaging of the tribofilm formation within the wear track were collected by using a HORIBA Lab RAM HR spectrometer (514 nm laser excitation) (HORIBA Jobin Yvon. FRANCE) and Raman 11 spectroscopy (Nanophonon. JAPAN). Prior to the characterization, the spectrometer calibration protocol was conducted based on the calibration routine proposed by Bocklitz et al.[46] This method ensures only Raman information of the sample was utilized by a chemometric model and exclude a contribution from artifacts from small shifts in the excitation wavelength. The deconvolution of peaks and the calculation of I_D/I_G were performed by using a Gaussian peak in Origin (Figure S15). The resulting data from areas, full width at half maximum (FWHM) and I_D/I_G ration was displayed in Table S2.

Nanoindentation Measurement: Elastic modulus and hardness of the tribofilm on the wear track were measured at the different regions by using Hysitron nanoindentation (TI-950 Triboindenter). In this study, a Berkovich diamond indenter (with 150 nm diameter) was used for all indentations. A high load (2 mN) indentation into the surface adjacent to the wear track was performed firstly to provide the information of the steel base for the comparison. The partial unload indentations to a maximum load of 500 μN with four segments per indentation was conducted in the smooth regions (graphene concentrated). To avoid the blunting of the indenter tip or formation of pile-ups, prior to each testing the geometric shape of the indenter tip was checked by using Field Emission Scanning Electron Microscopy (FE-SEM) (Dual Beam FEI Helios NanoLab G3 CX) to assure the testing accuracy. A constant normal load of 0.5 μN was typically used to *in-situ* imaging the topography of the wear surface. This allows us to choose the precise location to perform the indentation test on the aimed surface. The contact area of the indenter tip as a function of contact depth was calibrated by performing a partial unloading test into Quartz. The output data was used to calibrate the tip area function (A) of the system. The tip area function for the equipment is indicated below (9):

$$A= C_0h_c^2+C_1h_c+C_2h_c^{1/2}+C_3h_c^{1/4}+C_4h_c^{1/8}+C_5h_c^{1/16} \quad (9)$$

$$E_r=\frac{S\sqrt{\pi}}{2\sqrt{A}} \quad (10)$$

$$H = \frac{P}{A} \quad (11)$$

$$h_c=h_{max}-\varepsilon\frac{P_{max}}{S} \quad (12)$$

In each indent, the contact area (A_c) is determined and recorded via measuring the contact depth (h_c) (12). The elastic modulus (E_r) and the hardness (H) of the tribofilm were calculated by using Oliver and Pharr method via the equation (10) and (11). In the equations, S is the slope of the unloading (S = dP/dh) at the maximum displacement point (h_{max}), which can be derived from the force-displacement curve. P_{max} is the maximum load and P is the applied load. ε is the Sneddon's correction factor for the contact depth.

The Sneddon's coefficient can be in the range of 0.72 to 0.78 for the Berkovich indenter.[42] According to David et al.[43], the elastic modulus Er is a combination between the tribofilm and the indenter elastic deformation. To separate the indenter elastic deformation contribution, the equation (13) can be used:

$$E = \frac{1-\nu_s^2}{\frac{1}{E_r} - \frac{1-\nu_i^2}{E_i}} \qquad (13)$$

Where E and ν are the elastic modulus and Poisson's ratio of the materials being tested, and Ei and νi are from the indenter. In this studied, the Poisson's ratio was determined from the unloading curve using the method of Oliver and Pharr.[47]

Scanning Transmission Electron Microscopy: A Scanning Transmission Electron Microscope (STEM) (JEOL ARM 200F, Japan) was utilized to characterize the cross-sectional tribofilm on the wear track. Cross-sectional lamellar specimens were lifted out of the wear track using Focused Ion Meam mill (FIB) (Dual Beam FEI Helios NanoLab G3 CX) with a Gallium ion source. To support the investigation of elemental distribution across the wear track, lift-out specimens were also taken from regions perpendicular to the sliding direction on plates (Figure S6). Prior to FIB sectioning, a thin layer of carbon and platinum were deposited on the worn surface in order to protect the section from Ga ion beam damage. Electron energy loss spectroscopy (EELS) measurements were carried out using a GIF Quantum spectrometer (Gatan, Inc.) on the JEOL ARM 200F STEM. Electron Energy Loss Spectroscopy (EELS) images were recorded from regions of interest (ROI). In this study, the EELS technique enabled qualitative identification of carbon materials along with information on the bonding, based on relative intensities of the π* and σ* peaks of the carbon K edge.

The semi-quantification of sp^2 hybridization was performed via an integration window method.[48] Based on that, the ratio $I_{\pi^*}/(I_{\pi^*}+I_{\sigma^*})$ of C-K edge spectrum across the tribofilm was calculated by applying an energy window of 8 eV in the case of π* feartures and 15 eV for π*+σ* features. The sp^2-C bond fraction (%) was calculated according to the formula below (14):

$$\frac{sp^2}{sp^2+sp^3} = \frac{\frac{I^s_{\pi^*}}{I^s_{\pi^*}+I^s_{\sigma^*}}}{\frac{I^r_{\pi^*}}{I^r_{\pi^*}+I^r_{\sigma^*}}} \quad (14)$$

Where I^s represents the integrated intensities from the tribofilm sample, the reference sample of highly oriented pyrolytic graphite (100% sp^2-C bond) is denoted as I^r. The EELS spectrum data (Figure S16) was reproduced from Chen et al.[49] with permission from Nature Publishing Group. The referenced ratio $I_{\pi^*}/(I_{\pi^*}+I_{\sigma^*})$ was calculated as around 0.28 by applying an energy window of 8 eV in the case of π^* feartures and 15 eV for $\pi^*+\sigma^*$ features. Noted that, EELS spectrum was background subtracted using a Power Law fit model and then deconvoluted by the Fourier-ratio function using the simultaneously recorded zero-loss spectrum to remove the plural scattering effect. All the data processing was carried out in the Gatan DigitalMicrograph software.

Supporting Information

Supporting Information is available from the Wiley Online Library or from the author.

Acknowledgements

The study is funded by Australian Research Council (ARC) Discovery Project DP170103173. The authors acknowledge the use of the JEOL 6490 SEM at the UOW Electron Microscopy Centre.

The authours acknowledge the assisstance in using the FEI NanoLab G3 CX and JEOL JEM-ARM200F both funded by the Australian funded by the Australian Research Council (ARC) – Linkage, Infrastructure, Equipment and Facilities (LIEF) grants LE160100063 and LE120100104 respectively, located at the UOW Electron Microscopy Centre.

The authors acknowledge the assisstance of Dr. Christian Gow from Coherent Scientific Pty for using the TI-950 TriboIndenter to characterize the samples.

Received:

Revised:

Published online:

References

[1] a) S. Eigler, M. Enzelberger-Heim, S. Grimm, P. Hofmann, W. Kroener, A. Geworski, C. Dotzer, M. Röckert, J. Xiao, C. Papp, *Adv. Mater.* **2013**, 25, 3583; b) M. Alfè, V. Gargiulo, R. Di Capua, F. Chiarella, J.-N. Rouzaud, A. Vergara, A. Ciajolo, *ACS Appl. Mater. Interfaces.* **2012**, 4, 4491.

[2] M. Yi, Z. Shen, *J. Mater. Chem. A.* **2015**, 3, 11700.

[3] a) O. S. Panwar, A. Kumar Kesarwani, S. R. Dhakate, B. P. Singh, R. K. Rakshit, A. Bisht, S. Chockalingam, *J. Vac. Sci. Technol. B. Nanotechnol. Microelectron.* **2013**, 31, 040602; b) A. Kesarwani, O. Panwar, S. Dhakate, V. Singh, R. Rakshit, A. Bisht, A. Kumar, *Fuller. Nanotub. Car. N.* **2016**, 24, 725; c) O. Panwar, A. Kesarwani, S. Dhakate, B. Satyanarayana, *Vacuum.* **2018**, 153, 262.

[4] M. K. A. Ali, X. J. Hou, *Nanotechnol. Rev.* **2015**, 4, 347.

[5] D. Berman, A. Erdemir, A. V. Sumant, *Mater. Today.* **2014**, 17, 31.

[6] a) K.-S. Kim, H.-J. Lee, C. Lee, S.-K. Lee, H. Jang, J.-H. Ahn, J.-H. Kim, H.-J. Lee, *ACS Nano.* **2011**, 5, 5107; b) V. Khare, M.-Q. Pham, N. Kumari, H.-S. Yoon, C.-S. Kim, J.-I. Park, S.-H. Ahn, *ACS Appl. Mater. Interfaces.* **2013**, 5, 4063; c) J. Samuel, J. Rafiee, P. Dhiman, Z.-Z. Yu, N. Koratkar, *J. Phys. Chem. C.* **2011**, 115, 3410.

[7] a) H. Kinoshita, H. Ono, A. A. Alias, Y. Nishina, M. Fujii, *Mech. Eng.* **2015**, 2, 15; b) W. Zhang, M. Zhou, H. Zhu, Y. Tian, K. Wang, J. Wei, F. Ji, X. Li, Z. Li, P. Zhang, *J. Phys. D.* **2011**, 44, 205303; c) S. S. N. Azman, N. W. M. Zulkifli, H. Masjuki, M. Gulzar, R. Zahid, *J. Mater. Res.* **2016**, 31, 1932; d) J. Lin, L. Wang, G. Chen, *Tribol. Lett.* **2011**, 41, 209.

[8] V. Eswaraiah, V. Sankaranarayanan, S. Ramaprabhu, *ACS Appl. Mater. Interfaces.* **2011**, 3, 4221.

[9] a) J. M. Martin, *Tribol. Lett.* **1999**, 6, 1; b) R. Peason, *Chemical hardness: applications from molecules to solids*, Wiley-VCH: Weinheim, **1997**.

[10] W. Dai, B. Kheireddin, H. Gao, H. Liang, *Tribol. Int.* **2016**, 102, 88.

[11] a) P. U. Aldana, B. Vacher, T. Le Mogne, M. Belin, B. Thiebaut, F. Dassenoy, *Tribol. Lett.* **2014**, 56, 249; b) P. Rabaso, F. Ville, F. Dassenoy, M. Diaby, P. Afanasiev, J. Cavoret, B. Vacher, T. Le Mogne, *Wear.* **2014**, 320, 161.

[12] P. Rabaso, F. Dassenoy, F. Ville, M. Diaby, B. Vacher, T. Le Mogne, M. Belin, J. Cavoret, *Tribol. Lett.* **2014**, 55, 503.

[13] E. Hu, X. Hu, T. Liu, L. Fang, K. D. Dearn, H. Xu, *Wear.* **2013**, 304, 152.

[14] Y. Zhou, D. N. Leonard, H. M. Meyer, H. Luo, J. Qu, *Adv. Mater. Interf.* **2015**, 2, 1500213.

[15] O. J. Furlong, B. P. Miller, P. Kotvis, W. T. Tysoe, *ACS Appl. Mater. Interfaces.* **2011**, 3, 795.

[16] M. Woydt, J. Ebrecht, *Tribotest* **2008**, 14, 113.

[17] E. E. Hoffman, L. D. Marks, *Tribol. Lett.* **2016**, 63, 32.

[18] D. Berman, A. Erdemir, A. V. Sumant, *Carbon.* **2013**, 59, 167.

[19] Z. Ni, Y. Wang, T. Yu, Z. Shen, *Nano. Res.* **2008**, 1, 273.

[20] S. A. Shojaee, A. Zandiatashbar, N. Koratkar, D. A. Lucca, *Carbon.* **2013**, 62, 510.

[21] D. Uy, S. J. Simko, R. Carter III, R. K. Jensen, A. K. Gangopadhyay, *Wear* **2007**, 263, 1165.

[22] B. Yuan, W. Luan, S.-t. Tu, J. Wu, *New. J. Chem.* **2015**, 39, 3571.

[23] S. Berkani, F. Dassenoy, C. Minfray, J.-M. Martin, H. Cardon, G. Montagnac, B. Reynard, *Tribol. Lett.* **2013**, 51, 489.

[24] K. Ito, J. Martin, C. Minfray, K. Kato, *Tribol. T.* **2007**, 50, 211.

[25] X. Xu, D. Tang, J. Cai, B. Xi, Y. Zhang, L. Pi, X. Mao, *Appl. Catal. B-Environ.* **2019**, 251, 273.

[26] J. Roussel, A. Murray, J. Rolley, D. B. Johnson, L. Macaskie, presented at Advanced Materials Research **2015**.
[27] Y. Murooka, N. Tanaka, S. Hirono, M. Hibino, *Mater. Trans.* **2002**, 43, 2092.
[28] H. Spikes, *Tribol. Lett.* **2004**, 17, 469.
[29] a) A. Morina, A. Neville, M. Priest, J. Green, *Tribol. Int.* **2006**, 39, 1545; b) Z. Yin, M. Kasrai, G. Bancroft, K. Fyfe, M. Colaianni, K. Tan, *Wear.* **1997**, 202, 192; c) J. M. Martin, T. Onodera, M.-I. D. B. Bouchet, N. Hatakeyama, A. Miyamoto, *Tribol. Lett.* **2013**, 50, 95.
[30] Y. Lin, H. So, *Tribol. Int.* **2004**, 37, 25.
[31] A. Morina, A. Neville, *J. Phys. D.* **2007**, 40, 5476.
[32] Y.-B. Guo, S.-W. Zhang, *Lubricants.* **2016**, 4, 30.
[33] a) D. Berman, S. A. Deshmukh, S. K. Sankaranarayanan, A. Erdemir, A. V. Sumant, *Science*. **2015**, 348, 1118; b) P. Saravanan, R. Selyanchyn, H. Tanaka, D. Darekar, A. Staykov, S. Fujikawa, S. M. Lyth, J. Sugimura, *ACS Appl. Mater. Interfaces.* **2016**, 8, 27179; c) W. Kim, T. Lee, S. Han, *Carbon.* **2014**, 69, 55; d) D. Berman, B. Narayanan, M. J. Cherukara, S. K. Sankaranarayanan, A. Erdemir, A. Zinovev, A. V. Sumant, *Nat. Commun.* **2018**, 9, 1164.
[34] a) M. Rashad, F. Pan, A. Tang, M. Asif, *Pro. Nat. Sci-Mater.* **2014**, 24, 101; b) M. A. Rafiee, J. Rafiee, Z. Wang, H. Song, Z.-Z. Yu, N. Koratkar, *ACS Nano.* **2009**, 3, 3884.
[35] O. Panwar, A. Srivastava, S. Kumar, R. Tripathi, M. Kumar, S. Singh, *Surf. Coat. Technol.* **2011**, 206, 155.
[36] V. Dravid, X. Lin, Y. Wang, X. Wang, A. Yee, J. Ketterson, R. Chang, *Science.* **1993**, 259, 1601.
[37] a) S. Kandemir, *J. Mater. Eng. Perform.* **2018**, 1; b) M. Gürbüz, T. Mutuk, *J. Compos. Mater.* **2018**, 52, 543; c) Z. Hu, G. Tong, D. Lin, C. Chen, H. Guo, J. Xu, L. Zhou, *Mater. Sci. Technol.* **2016**, 32, 930.
[38] Y. Cao, X. Luo, H. Yu, F. Peng, H. Wang, G. Ning, *Catal. Sci. Technol.* **2013**, 3, 2654.
[39] L. Zhang, Q. Xu, J. Niu, Z. Xia, *Phys. Chem. Chem. Phys.* **2015**, 17, 16733.
[40] J. D. Burrington, J. K. Pudelski, J. P. Roski, in *Practical Advances in Petroleum Processing*, Springer **2006**, p. 579.
[41] A. Bianco, H.-M. Cheng, T. Enoki, Y. Gogotsi, R. H. Hurt, N. Koratkar, T. Kyotani, M. Monthioux, C. R. Park, J. M. Tascon, Elsevier, 2013.
[42] X. Dou, A. R. Koltonow, X. He, H. D. Jang, Q. Wang, Y.-W. Chung, J. Huang, *Proc. Natl. Acad. Sci. U.S.A.* **2016**, 113, 1528.
[43] a) A. Ferrari, J. Robertson, *Phys. Rev. B.* **2001**, 64, 075414; b) I. Calizo, A. Balandin, W. Bao, F. Miao, C. Lau, *Nano. Lett.* **2007**, 7, 2645.
[44] S. Ferguson, J. Johnson, D. Gonzales, C. Hobbs, C. Allen, S. Williams, *Phys. Procedia.* **2015**, 66, 439.
[45] B. J. Hamrock, D. Dowson, *J. Lubr. Technol.* **1977**, 99, 264.
[46] T. Bocklitz, T. Dörfer, R. Heinke, M. Schmitt, J. Popp, *Spectrochim. Acta. A* **2015**, 149, 544.
[47] W. C. Oliver, G. M. Pharr, *J. Mater. Res.* **1992**, 7, 1564.
[48] S. Berger, D. McKenzie, P. Martin, *Philos. Mag.* **1988**, 57, 285.
[49] X. Chen, C. Zhang, T. Kato, X.-a. Yang, S. Wu, R. Wang, M. Nosaka, J. Luo, *Nat. Commun.* **2017**, 8, 1675.

Note edited figures provided in separate copy

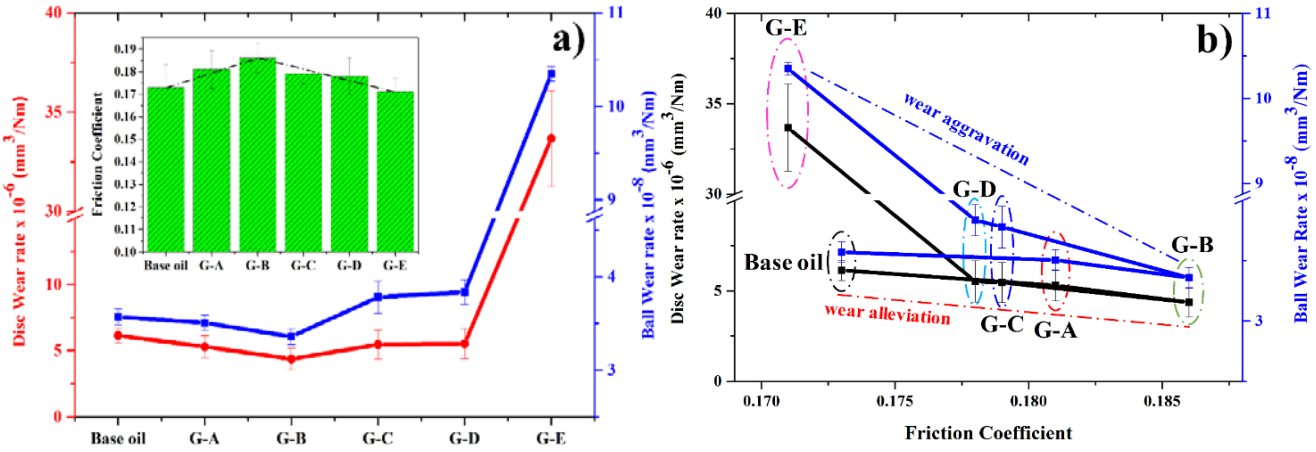

Figure 1. a) Specific wear rate as a function of GNP concentrations added into formulated engine oil. The inset graph in a) is a corresponding friction coefficient; b) Wear rates plotted as a function of friction coefficient for engine oil containing various amounts of graphene: base oil (graphene-free); G-A (0.01 wt.%); G-B (0.05 wt.%); G-C (0.1 wt.%); G-D (0.2 wt.%); and G-E (0.5 wt.%).

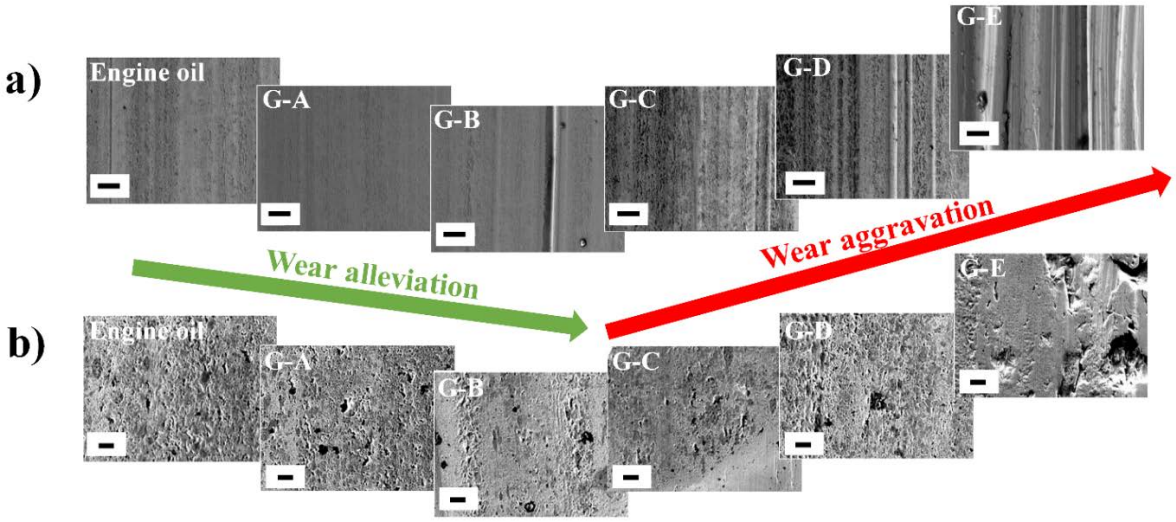

Figure 2. SEM secondary electron images showing the morphology of wear scars on both plate a) and corresponding ball b) after tribo-testing with various oil samples: commercial engine oil (graphene-free); G-A (0.01 wt.% graphene); G-B (0.05 wt.% graphene); G-C (0.1 wt.% graphene); G-D (0.2 wt.% graphene); and G-E (0.5 wt.% graphene). The scale bar in a) is 50 μm and in b) is 10 μm.

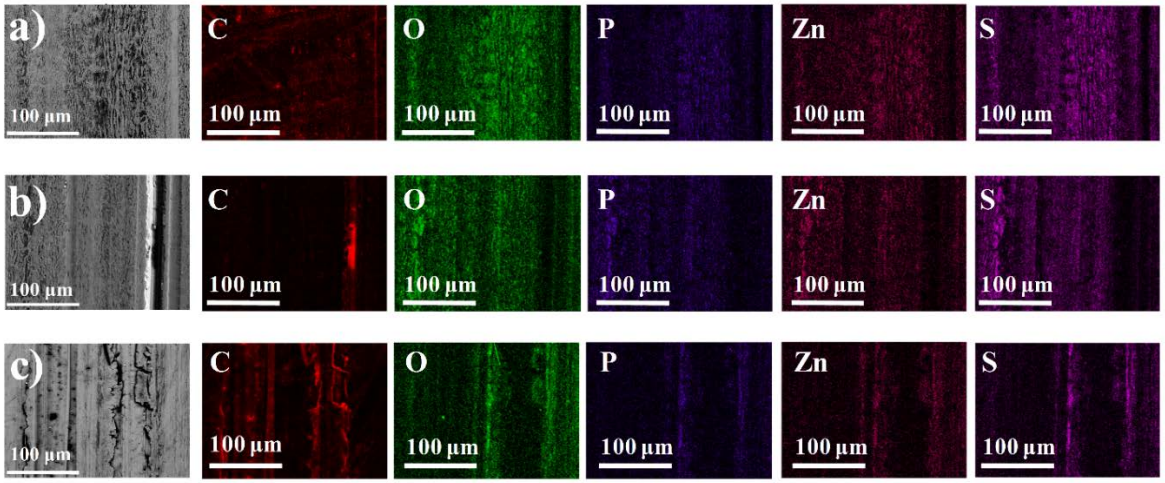

Figure 3. EDS mapping across the disc wear track of: a) engine oil (graphene-free) lubricant; b) G-B (0.05 wt. % graphene concentration) lubricant; and c) G-E (0.5 wt. % graphene concentration) lubricant.

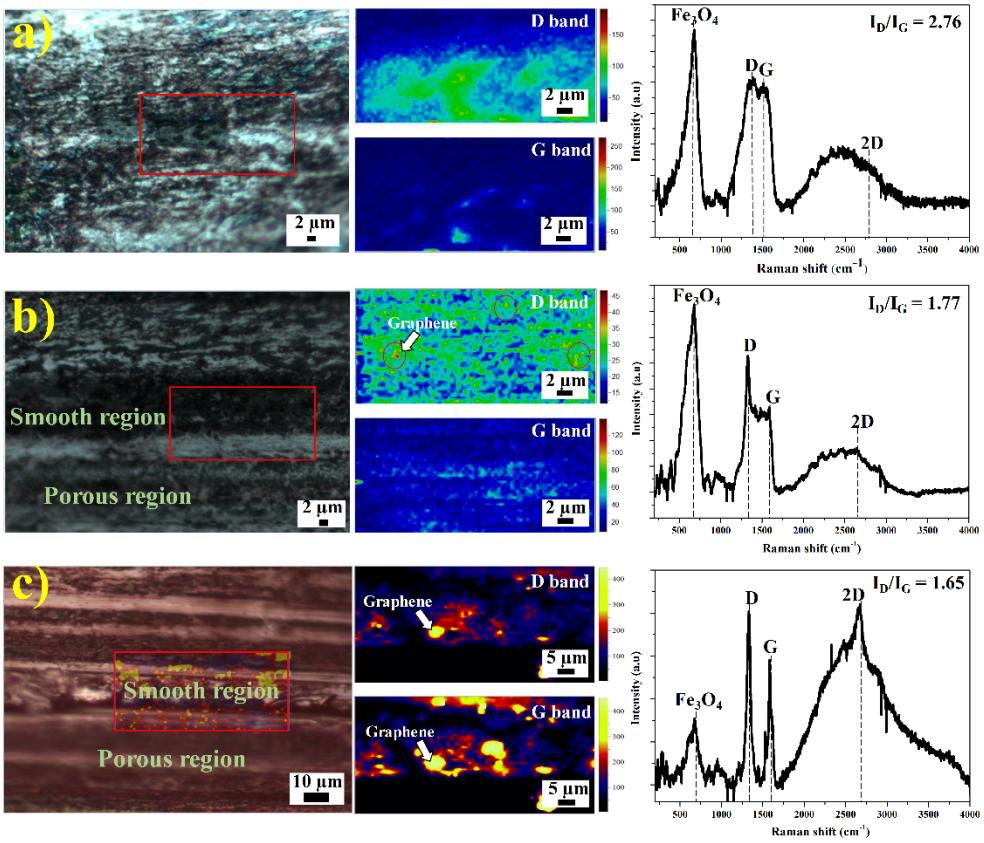

Figure 4. Raman mapping and Raman imaging of tribofilm on the wear track after test of a) commercial engine oil (graphene-free); b) G-B (0.05 wt.% graphene); and c) G-E (0.5 wt.% graphene) test lubricants.

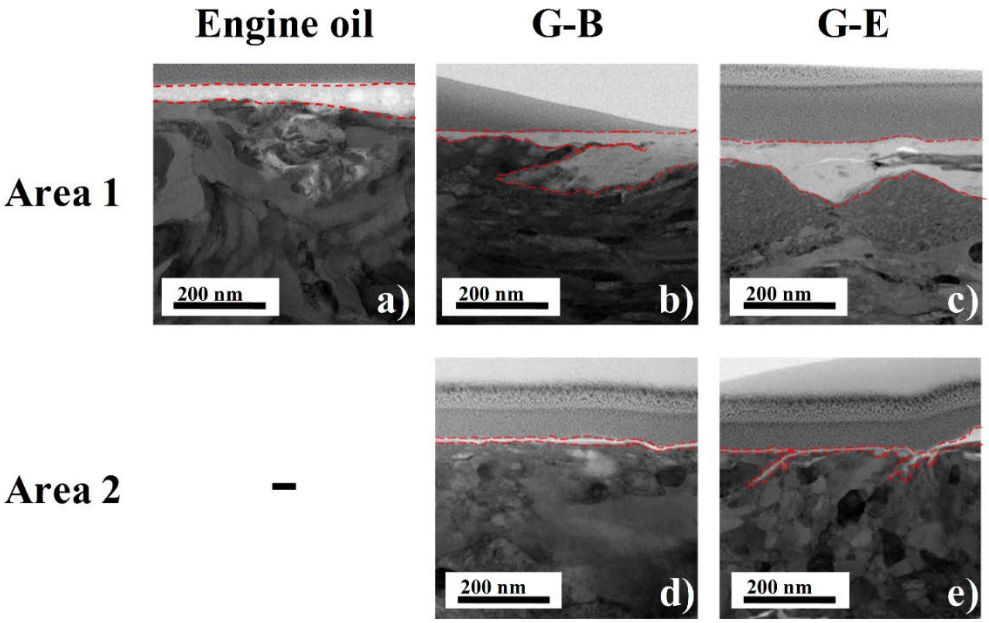

Figure 5. STEM bright field images of tribofilm formation at the surface in two different regions: Area 1 is from porous regions of wear scar with a high concentration of ZDDP: a) base engine oil (graphene-free); b) G-B (0.05 wt.% graphene); and c) G-E (0.5 wt.% graphene). Area 2 is from smooth regions of wear scar with a high concentration of carbon and low concentration of ZDDP: d) G-B; and e) G-E.

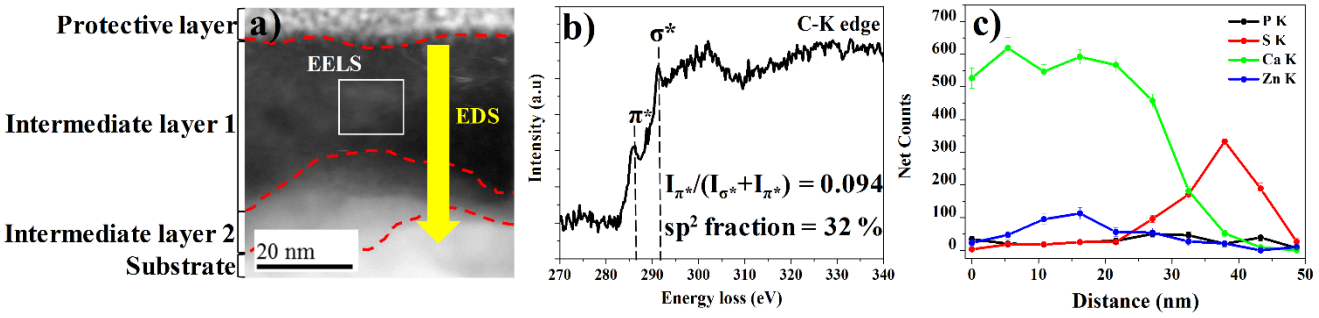

Figure 6. a) Highly magnified STEM-HADDF spectrum of the hierrachical tribofilm structure from graphene-free engine oil; b) EELS spectrum of the tribofilm from the white box in a) showing the calculated $I_{\pi^*}/(I_{\pi^*}+I_{\sigma^*})$ ratio of amorphous carbon; and c) EDS line profile analysis across the tribofilm from the yellow arrow in a).

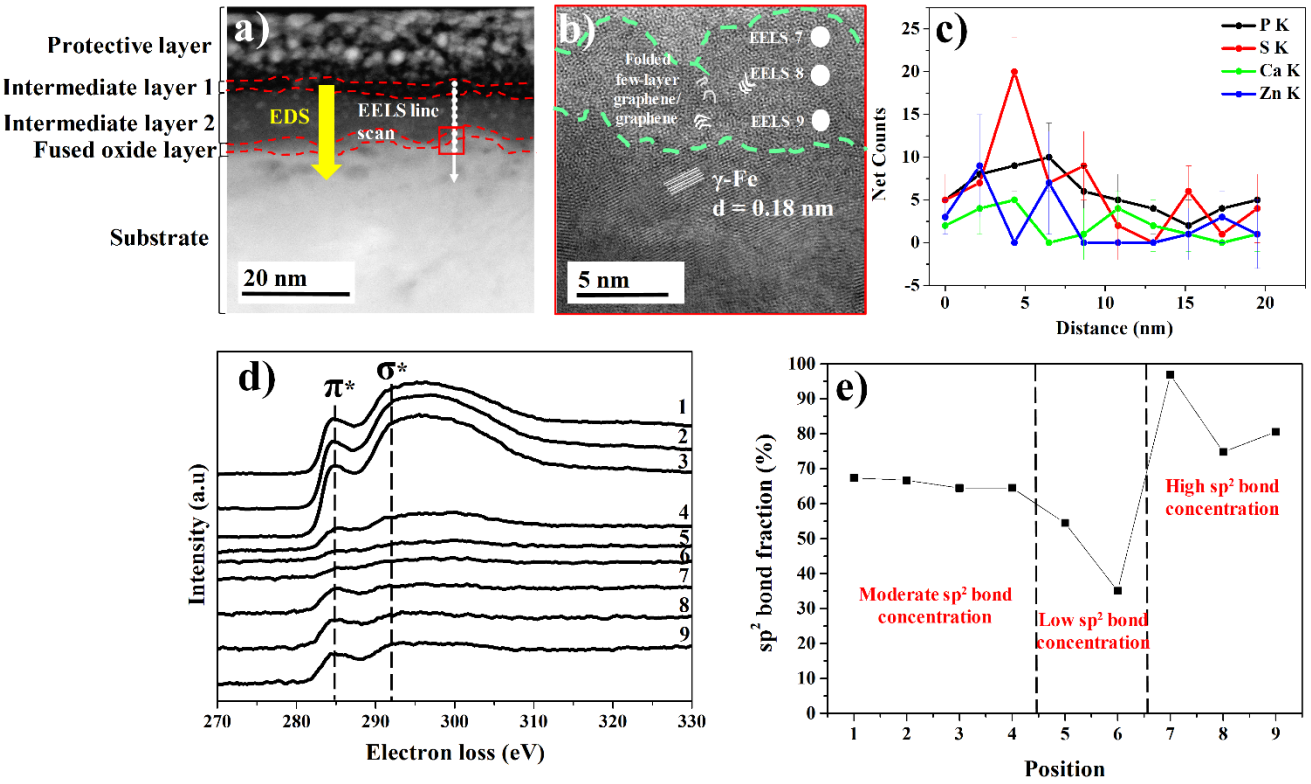

Figure 7. a) HADDF imaging of multi-layered thin tribofilm derived from test G-B (0.05 wt.% graphene concentration) lubricant; b) STEM-BF detail of the fused oxide tribofilm - red boxed region in a); c) EDS line scane across the tribofilm marked by yellow arrow in a); d) EELS C K edge spectra along the line profile marked by white dots in a); and e) Calculated $I_{\pi^*}/(I_{\pi^*}+I_{\sigma^*})$ ratio in different spots from d) showing the variation of the sp^2 coordination of carbon across the tribofilms regions.

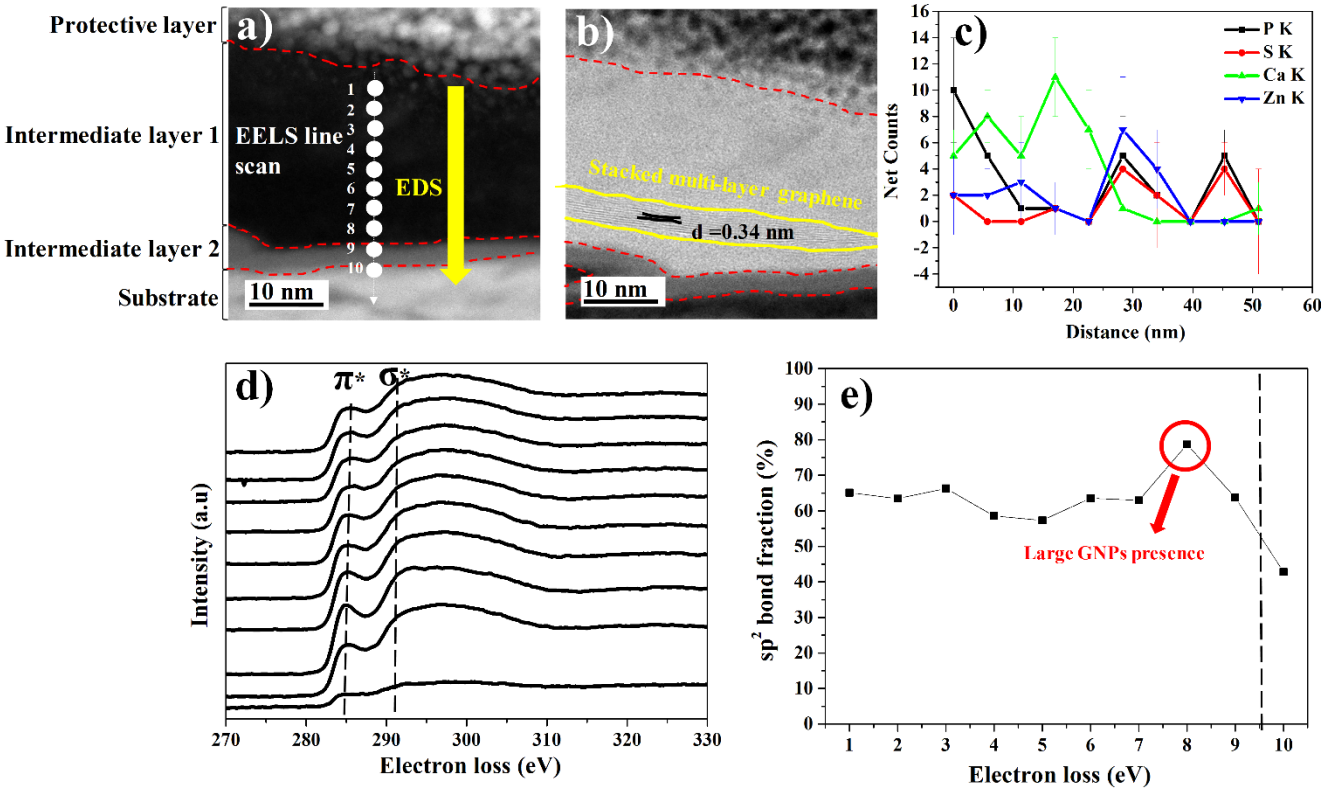

Figure 8. a) HADDF imaging of the multi-layered tribofilm derived from test G-E (0.5 wt.% graphene concentration) lubricant; b) STEM-BF imaging of the tribofilm with the presence of stacked graphene nanosheets; c) EDS line scane across the tribofilm as yellow arrow marked in a); d) EELS C K edge spectra across the tribofilm along the line profile marked by white dots in a); and e) Calculated $I_{\pi^*}/(I_{\pi^*}+I_{\sigma^*})$ ratio from the spectra in (d) showing the change of sp^2 coordination of carbon across the tribofilm.

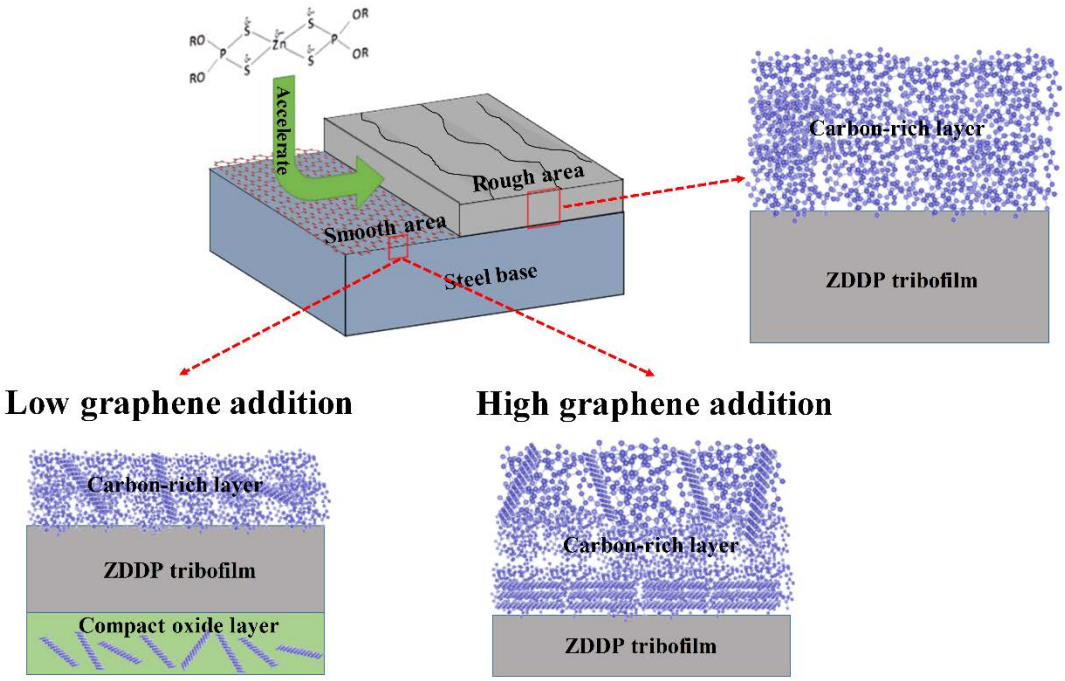

Figure 9. Schematic of hierarchical tribofilm structure derived from different test lubricants: graphene-free engine oil, test G-B (0.05 wt.% graphene concentration) and test G-E (0.5 wt.% graphene concentration) lubricants showing the change in nature of the tribofilm formation.

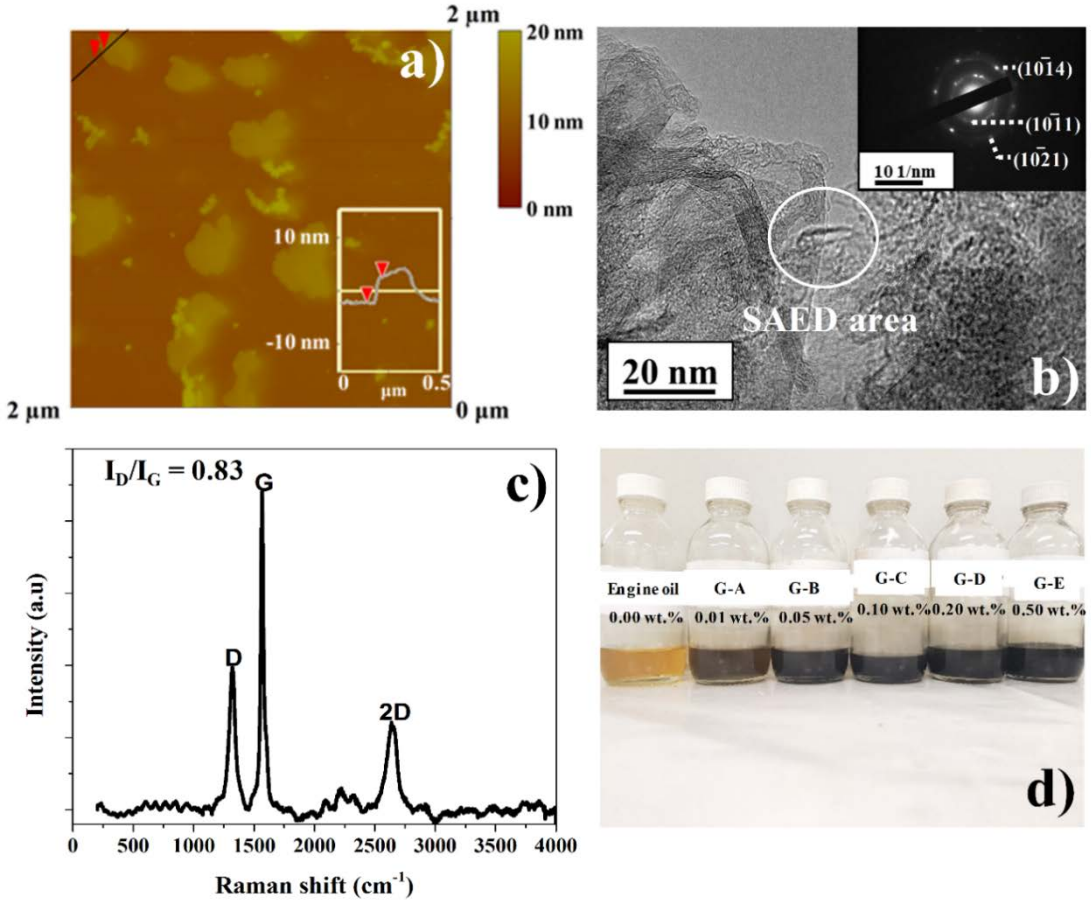

Figure 10. a) AFM image of GNP; b) TEM bright field image of GNP. The inset picture in b) is a SADP of crystalline GNP; c) Raman spectrum of GNP with the peak ratios are consistent with graphene; and d) Lubricant samples with different concentration of GNP after one week of dispersion.

Table 1. *Composition of steel ball and steel plate.*

Material	Composition (wt. %)
Steel Plate	0.08 %C, 2 %Mn, 0.75 %Si, 0.045 %P, 0.030 %S, 18 %Cr, 8 %Ni
Steel Ball	0.08 %C, 2 %Mn, 0.75 %Si, 0.045 %P, 0.030 %S, 16 %Cr, 10 %Ni, 2 %Mo